

Article

Not peer-reviewed version

Palladium-Rhenium Catalysts for Selective Hydrogenation of Furfural: Influence of Catalyst Preparation on Structure and Performance

Simon T. Thompson and [Henry H. Lamb](#) *

Posted Date: 25 July 2023

doi: 10.20944/preprints2023071556.v1

Keywords: bimetallic catalyst; Raman spectroscopy; TPR; palladium hydride; chemisorption; DRIFTS; STEM-EDX



Preprints.org is a free multidiscipline platform providing preprint service that is dedicated to making early versions of research outputs permanently available and citable. Preprints posted at Preprints.org appear in Web of Science, Crossref, Google Scholar, Scilit, Europe PMC.

Copyright: This is an open access article distributed under the Creative Commons Attribution License which permits unrestricted use, distribution, and reproduction in any medium, provided the original work is properly cited.

Article

Palladium-Rhenium Catalysts for Selective Hydrogenation of Furfural: Influence of Catalyst Preparation on Structure and Performance

Simon T. Thompson and H. Henry Lamb *

Department of Chemical and Biomolecular Engineering, North Carolina State University, Raleigh, NC 27695-7905, USA

* Correspondence: lamb@ncsu.edu; Tel.: +01-919-515-6395

Abstract: PdRe/Al₂O₃ catalysts are highly selective for hydrogenation of furfural to furfuryl alcohol (FAL). Moreover, synergy between the metals can result in greater specific activity (higher turnover frequency, TOF) than exhibited by either metal alone. Bimetallic catalyst structure depends strongly on the metal precursors employed and their addition sequence to the support. In this work, PdRe/Al₂O₃ catalysts were prepared by: (i) co-impregnation (CI) and sequential impregnation (SI) of γ -Al₂O₃ using HReO₄ and Pd(NO₃)₂, (ii) SI using NH₄ReO₄ and [Pd(NH₃)₄(NO₃)₂], (iii) HReO₄ addition to a reduced and passivated Pd/Al₂O₃ catalyst, and (iv) impregnation with the double complex salt (DCS), [Pd(NH₃)₄(ReO₄)₂]. Raman spectroscopy and temperature-programmed reduction (TPR) evidence larger supported PdO crystallites in catalysts prepared using Pd(NO₃)₂ than [Pd(NH₃)₄(NO₃)₂]. Surface [ReO₄]⁻ species detected by Raman exhibit TPR peak temperatures from ranging 85 to 260°C (versus 375°C for Re/Al₂O₃). After H₂ reduction at 400°C, the catalysts were characterized by chemisorption, temperature-programmed hydride decomposition (TPHD), CO diffuse reflectance infrared Fourier transform spectroscopy (DRIFTS), and scanning transmission electron microscopy (STEM) with energy-dispersive x-ray (EDX) spectroscopy. The CI catalyst containing supported Pd-Re alloy crystallites had a TOF similar to Pd/Al₂O₃ but higher (61%) FAL selectivity. In contrast, catalysts prepared by methods (ii-iv) containing supported Pd-Re nanoparticles exhibit higher TOFs and up to 78% FAL selectivity.

Keywords: bimetallic catalyst; Raman spectroscopy; TPR; palladium hydride; chemisorption; DRIFTS; STEM-EDX

1. Introduction

Rhenium is used in supported bimetallic catalysts with other Group VIII metals (such as Rh [1–4], Ru [5,6] and Pd [7]) to enhance selective hydrogenation and hydrogenolysis of oxygenated organic compounds. Tomishige and coworkers investigated SiO₂- and C-supported Re bimetallic catalysts for a variety of reactions, including ester hydrogenolysis [2], ring-opening of cyclic ethers [1,4], hydrogenation of fatty acids to alcohols [7], and glycerol hydrogenolysis [8]. For each reaction, Re addition boosts activity and selectivity to the desired product, e.g., 1,5-pentanediol from ring-opening of tetrahydrofurfuryl alcohol [4]. Similarly, Re addition to Pd/SiO₂ increased selectivity to fatty alcohols in fatty acid hydrogenation [7]. Suppression of CO chemisorption (compared to Rh/SiO₂) and the observed modification of catalytic activity suggested surface modification of supported Rh particles by Re species. Complementary results from extended x-ray absorption fine structure (EXAFS) spectroscopy, x-ray photoelectron spectroscopy (XPS), x-ray diffraction, and scanning transmission electron microscopy with energy-dispersive x-ray analysis (STEM-EDX) led to the conclusion that low-valent ReO_x species in contact with supported Rh particles were the active sites [4,9]. Supported PdRe catalysts also have been investigated for selective hydrogenation of dicarboxylic acids [10–12], hydrodechlorination [13,14], and reforming reactions [15].

Structural investigations of PdRe/Al₂O₃ catalysts have been limited. Meitzner, et al. examined a 0.6 wt.% Pd-1 wt.% Re/Al₂O₃ catalyst prepared by incipient wetness (IW) co-impregnation (CI) by EXAFS spectroscopy and inferred Pd-Re alloy formation [16]. Ziemecki, et al. investigated PdRe/Al₂O₃ catalysts prepared by sequential impregnation (SI): depositing a Pd²⁺ salt on \ominus -Al₂O₃, calcining, reducing to Pd⁰, passivating, and then adding the Re precursor [17,18]. Characterization of the resultant catalyst by temperature-programmed reduction (TPR), H₂ uptake measurements and *in situ* x-ray diffraction (XRD) demonstrated that substitutional alloying with Re was responsible for suppression of bulk palladium hydride (PdH_x) formation. Karpinski and coworkers used a similar preparation method and also reported PdH_x suppression associated with PdRe alloy formation based on XRD and temperature-programmed hydride decomposition (TPHD) [13–15]. Because the addition of small amounts of Re to Pd/Al₂O₃ suppressed CO chemisorption and inhibited hydroisomerization activity, they concluded that Re occupied the surface of Pd-rich alloy particles [14]. More recently, Holles and coworkers used directed deposition to selectively form Pd overlayers on alumina-supported Re particles [19,20]; the catalysts were characterized primarily by H₂ chemisorption and a simple probe reaction (ethylene hydrogenation).

Our previous research on PdRe/Al₂O₃ catalysts for selective hydrogenation of furfural to furfuryl alcohol (FAL) demonstrated substantial differences in catalyst structure and performance depending on the preparation method, metal precursors, and Pd:Re ratio [21]. A strong correlation between selective hydrogenation activity and suppression of H₂ chemisorption was observed. The H/CO chemisorption ratio at 35°C correlated with furfuryl turnover frequency (TOF) and FAL selectivity, and there was an optimum surface composition. PdRe/Al₂O₃ catalysts with 1:2 Pd:Re molar ratios (exhibiting very low H/CO ratios) had low activity suggesting that the Pd surface was covered by Re. More recently, Kammert, et al. investigated PdRe/SiO₂ and PdRe/TiO₂ catalysts for hydrogenation of propionic acid and proposed that Pd facilitates the reaction by dissociating H₂ providing hydrides and protons to vicinal Re sites [22].

In this work, we further elucidate the structures of PdRe/Al₂O₃ catalysts for selective hydrogenation of furfural using TPR, TPHD, CO and H₂ chemisorption, CO diffuse reflectance infrared Fourier transform spectroscopy (DRIFTS), and STEM-EDX. The roles of the metal precursors, impregnation sequence, and calcination conditions in determining catalyst morphology (i.e., particle size and metal-metal interactions) are investigated. Moreover, we take advantage of the strong Raman bands of the perrhenate ion, [ReO₄]⁻, and PdO crystallites to characterize the as-prepared catalysts. Otto, et al. measured the Raman spectra of a series of Pd/Al₂O₃ catalysts and found a linear relationship between the intensity of the PdO B_{1g} lattice vibration and Pd loading (up to 2.5 wt.%) [23]. Baylet, et al. used *in situ* Raman spectroscopy to investigate the dynamics of Pd/Al₂O₃ oxidation catalysts [24]. Re/Al₂O₃ catalysts have been probed extensively by Raman spectroscopy [25–27], but we are not aware of any studies of PdRe/Al₂O₃ catalysts. To facilitate Raman spectroscopy, a new series of PdRe/Al₂O₃ catalysts was prepared using a \ominus -Al₂O₃ support that did not fluoresce strongly in the region of interest. Specifically, catalysts were prepared by: (i) CI and SI of γ -Al₂O₃ using HReO₄ and Pd(NO₃)₂, (ii) SI using NH₄ReO₄ and [Pd(NH₃)₄(NO₃)₂] (intermediate and final calcination steps), (iii) SI via HReO₄ addition to a reduced and passivated Pd/Al₂O₃ catalyst, and (iv) impregnation with the double complex salt (DCS), [Pd(NH₃)₄(ReO₄)₂].

2. Results and Discussion

2.1. Catalyst Characterization

The catalysts, metal precursors and loadings are listed in Table 1. The catalyst name denotes the metal(s), target loading(s) (wt.%), and metal precursor(s): nitrate, N or tetraammine nitrate, TA for Pd, and perrhenic acid, H or ammonium perrhenate, N for Re. Co-impregnation and sequential impregnation are indicated by CI and SI, respectively. The impregnation sequence (for SI) is indicated by the order of metals (e.g., Re-first 5 wt.%, Pd 3 wt.% = Re5Pd3). DCS indicates impregnation with the stoichiometric double complex salt, [Pd(NH₃)₄(ReO₄)₂].

Table 1. Precursors and compositions of γ -Al₂O₃-supported catalysts.

Catalyst	Metal precursor(s)	Pd loading (wt%)	Re loading (wt%)
Pd1-N	Pd(NO ₃) ₂	0.91	---
Pd3-N	Pd(NO ₃) ₂	2.66	---
Pd3-TA	Pd(NH ₃) ₄ (NO ₃) ₂	2.34	---
Pd3Re5-CI	Pd(NO ₃) ₂ and HReO ₄	2.43	4.41
Pd3Re5-SI	Pd(NH ₃) ₄ (NO ₃) ₂ and HReO ₄	2.80	4.63
Re5Pd3N-SI	HReO ₄ and Pd(NO ₃) ₂	2.15	5.73
Re5Pd3-SI (350)	NH ₄ ReO ₄ and Pd(NH ₃) ₄ (NO ₃) ₂	2.56	4.23
Re5Pd3-SI	NH ₄ ReO ₄ and Pd(NH ₃) ₄ (NO ₃) ₂	2.27	4.24
Re5Pd1.5-DCS	Pd(NH ₃) ₄ (ReO ₄) ₂	1.42	4.65
Re5-H	HReO ₄	---	5.29
Re5-N	NH ₄ ReO ₄	---	4.54

Raman spectra of the as-prepared 3 wt.% Pd/Al₂O₃ catalysts (Figure 1a) contain a peak at \sim 640 cm⁻¹ corresponding to the B_{1g} lattice vibration of PdO crystallites [28]. This peak has negligible intensity in the Raman spectrum of the as-prepared Pd1-N catalyst (not shown). It has been observed at 626 to 651 cm⁻¹ in supported Pd catalysts and PdO thin films [23,24,29–31]. A weak Raman peak at \sim 280 cm⁻¹ is also observed that was attributed by McBride, et al. to a second-order scattering process [28]. Another Raman band at 445 cm⁻¹ was assigned to the E_g lattice vibration; however, McBride, et al. note that the band is extremely weak when employing 632.8 nm (He-Ne laser) excitation [28]. Otto, et al. [23] found that the integrated intensity of the B_{1g} lattice vibration was directly proportional to Pd loading (0.2–2.5 wt.% range) in fully oxidized Pd/Al₂O₃ catalysts. They suggested that highly dispersed PdO crystallites smaller than \sim 1.5 nm (containing fewer than ca. 50 metal atoms) interacting with the γ -Al₂O₃ support were undetectable by Raman spectroscopy.

Despite their similar Pd loadings, the Raman B_{1g} band of Pd3-N is much stronger and shifted slightly to lower wavenumbers than that of Pd3-TA leading us to infer that the Pd3-N catalyst contains larger PdO crystallites. The smaller PdO particle size (i.e., higher dispersion) achieved using the tetraammine nitrate precursor can be explained by strong electrostatic adsorption (SEA) [32]. The pH of the [Pd(NH₃)₄(NO₃)₂] impregnation solution was well above the point-of-zero charge (PZC) of γ -Al₂O₃ (8.0 ± 0.2) resulting in a net negative charge on the support. Specifically, surface hydroxyl groups are deprotonated leaving surface O[–] ions that electrostatically attract [Pd(NH₃)₄]²⁺ cations. In contrast, Pd(NO₃)₂ solutions are neutral to slightly acidic (pH below PZC of γ -Al₂O₃), and the SEA effect is negated.

Raman spectra of the as-prepared Re/Al₂O₃ catalysts (Figure 1a) contain peaks corresponding to rhenium-oxygen stretching and bending modes. The strong sharp peak at 970 cm⁻¹ is assigned to the symmetric Re=O stretching mode (v_s) of T_d [ReO₄][–] species [25–27]. The peak position corresponds to perrhenate ion in aqueous solution, as expected following exposure to ambient moisture. Additional bands at 920 (vw) and 335 (w) cm⁻¹ are assigned to the antisymmetric Re=O stretching (v_{as}) and O-Re-O bending (δ) modes, respectively. Significantly, no Raman bands indicative of Re–O–Re bonding are observed consistent with submonolayer coverage of isolated perrhenate species on γ -Al₂O₃. A small peak appears at 1000 cm⁻¹ in the Raman spectrum of Re5-H. The symmetric Re=O stretching peak is shifted to \sim 1000 cm⁻¹ for a hypothetical C_{3v} [ReO₄] species with three identical Re=O bonds and a Re–O–Al bridge to the support [25,33]; however, this species typically is found only under dehydrated conditions [26,27].

The strong PdO band (B_{1g} mode) in the Raman spectrum of Pd3Re5-CI evidences that PdO crystallites are present following calcination (Figure 1b). A strong shoulder at \sim 550 cm⁻¹ and a weak band at \sim 280 cm⁻¹ are also observed. A medium-intensity v_s(Re=O) band at \sim 1000 cm⁻¹ and weak δ (O–Re–O) band at 335 cm⁻¹ are observed consistent with isolated [ReO₄][–] species. An unassigned weak broad feature at \sim 850 cm⁻¹ is also noted. The Raman spectrum of Re5Pd3N-SI, another bimetallic catalyst prepared from Pd(NO₃)₂, is closely similar. Qualitatively, the v_s(Re=O) bands for these bimetallic catalysts are broader and less intense than those for Re5-H and Re5-N (Figure 1a). The

strong intensity of the B_{1g} mode is indicative of supported PdO crystallites. The medium-intensity $\nu_s(\text{Re}=\text{O})$ band contains at least two components between 1000 and 970 cm^{-1} indicating $[\text{ReO}_4]^-$ species in different environments.

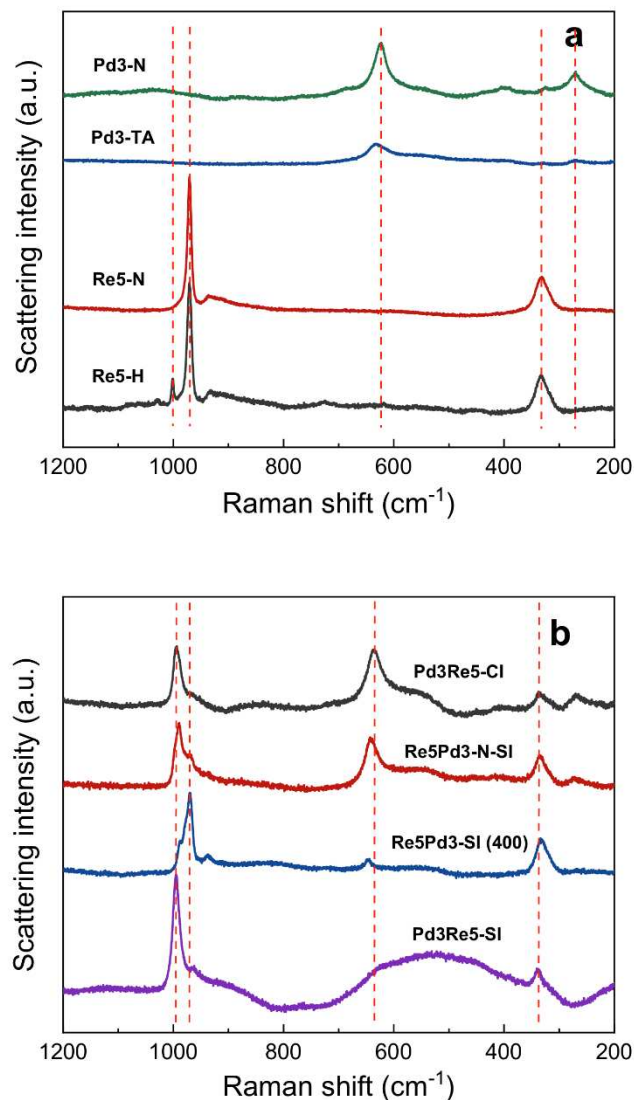
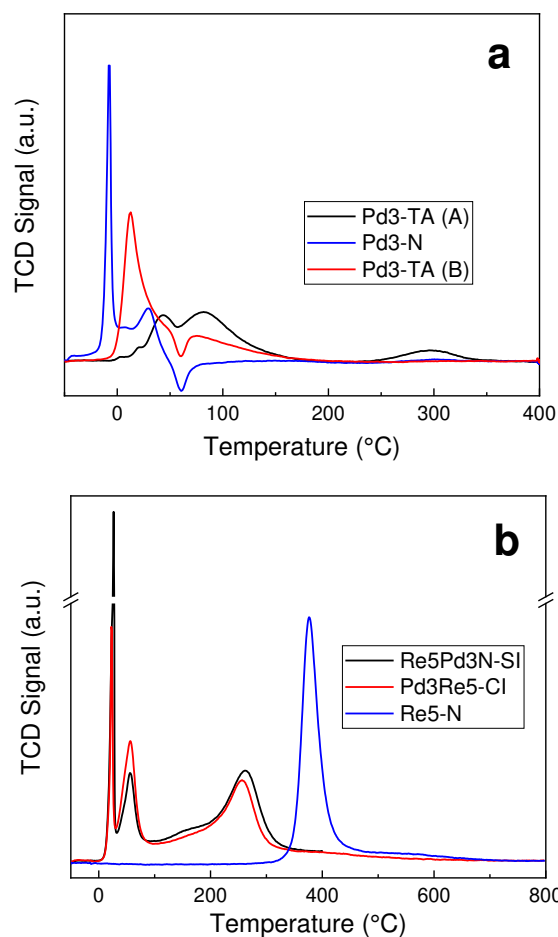


Figure 1. Raman spectra of Pd/ Al_2O_3 and Re/ Al_2O_3 catalysts (a) and PdRe/ Al_2O_3 catalysts (b).

In contrast, the PdO B_{1g} mode in the Raman spectrum of Re5Pd3-SI (Figure 1b) is very weak and shifted to slightly higher wavenumbers indicating that only small PdO nanoparticles and/or isolated Pd oxo complexes are present after the final calcination. These results suggest that the size and distribution of PdO particles after calcination is affected more strongly by the metal precursor than by the method of preparation. We infer that SEA of the tetraammine complex to the ReO_x -modified support results in highly dispersed Pd oxo species. A strong $\nu_s(\text{Re}=\text{O})$ peak is observed at 970 cm^{-1} with a shoulder at $\sim 1000 \text{ cm}^{-1}$. The $\nu_{as}(\text{Re}=\text{O})$ and $\delta(\text{O}-\text{Re}-\text{O})$ peaks at 920 and 335 cm^{-1} , respectively, allow a definitive assignment to T_d $[\text{ReO}_4]^-$. The PdO B_{1g} band has negligible intensity in the Raman spectrum of Pd3Re5-SI (Figure 1b). Instead, a large, broad feature at 300-700 cm^{-1} due to fluorescence from the γ - Al_2O_3 support is observed. Otto, et al. inferred that fluorescence in this region is quenched by a PdO-support interaction [23]. Consistent with this hypothesis, fluorescence is suppressed for the other catalysts examined herein. In Pd3Re5-SI, Pd was reduced and passivated prior to impregnation with H ReO_4 . The absence of a low-temperature TPR peak (*vide infra*) indicates that the Pd^0 particles are not converted to bulk PdO, and we infer that a thin Pd O_x layer is formed consistent with the

oxidation mechanism proposed by Su, et al. [29]. The strong Raman band at 1000 cm^{-1} is assigned to $[\text{ReO}_4^-]$ species interacting with support and/or the PdO_x -covered metal particles.

TPR profiles of the as-prepared 3% Pd/ AlO_3 catalysts are shown in Figure 2a. Reduction of larger supported PdO crystallites in Pd3-N occurs abruptly at sub-ambient temperatures resulting in a very sharp H_2 uptake peak at approximately -10°C . An additional H_2 uptake feature at $\sim 30^\circ\text{C}$ is ascribed to reversible PdH_x formation; H_2 evolution associated with PdH_x decomposition is observed at $\sim 55^\circ\text{C}$. TPR profiles of two Pd3-TA catalysts (A and B) prepared using different alumina supports are also shown. The TPR profile for Pd3-TA (A) (prepared using the same support as the other catalysts in this work) is broader and reduction occurs at higher temperatures consistent with PdO nanoparticles interacting strongly with the $\gamma\text{-Al}_2\text{O}_3$ support and/or surface-bound Pd oxo complexes. There is a shallow dip in the TCD signal at $\sim 55^\circ\text{C}$ consistent with PdH_x decomposition followed by a broad maximum at $\sim 80^\circ\text{C}$. The small H_2 consumption feature at 290°C arises from reduction of carbonate species associated with alkali and alkaline impurities, as confirmed by CH_4 evolution [34]. In contrast, H_2 consumption during TPR of Pd3-TA (B) occurs primarily at $< 50^\circ\text{C}$. Because Pd^0 particles are formed at low temperature, H_2 is evolved at 55°C (inverse peak) due to $\beta\text{-PdH}_x$ decomposition. H_2 uptake continues to $\sim 200^\circ\text{C}$. Because $\gamma\text{-Al}_2\text{O}_3$ (B) lacks the alkali and alkaline metal impurities of $\gamma\text{-Al}_2\text{O}_3$ (A), a H_2 uptake feature at 290°C is not observed. Quantitative H_2 uptake measurements [excluding the 290°C peak for Pd3-TA (A)] (Table 2) indicate complete reduction of Pd^{2+} to Pd^0 following TPR to 400°C . The TPR profile of Re5-N (Figure 2b) contains a well-defined peak at 375°C with a high-temperature tail extending to $\sim 700^\circ\text{C}$. TPR peak position and shape for Re5-H are similar (not shown). Quantitative H_2 uptake measurements (Table 2) indicate incomplete reduction of Re^{7+} after TPR to 400°C ; however, complete reduction to Re^0 was achieved after TPR to 800°C .



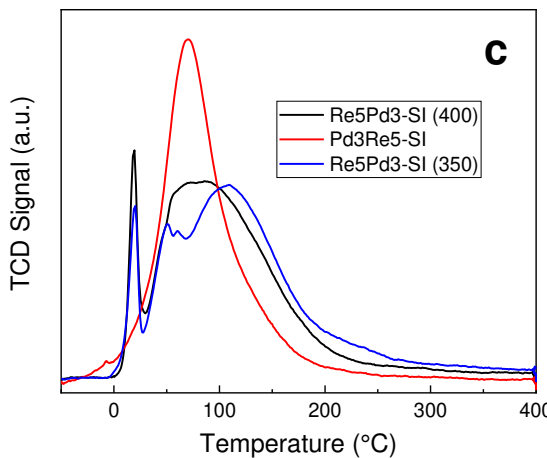


Figure 2. TPR profiles of $\text{Pd}/\text{Al}_2\text{O}_3$, $\text{Re}/\text{Al}_2\text{O}_3$, and $\text{PdRe}/\text{Al}_2\text{O}_3$ catalysts. Pd3-N (**b**) is described in [21].

Table 2. TPR and TPHD results for selected catalysts.

Catalyst	H/metal ratio (TPR) ¹	Re oxidation state (TPR) ²	H/Pd (TPHD) ⁴
Pd3-N	2.1	--	0.32
Pd3-TA	2.4	--	0.13
Pd3Re5-CI	4.4	0.4	0.063
Pd3Re5-SI	3.6	0.7 ³	0.058
Re5Pd3N-SI	5.0	0.7	0.18
Re5Pd3-SI (350)	4.3	0.3	0.11
Re5Pd3-SI	4.5	0.2	0.12
Re5-N	4.9	2.1	--

¹ Based on TPR H_2 consumption to 400°C. ² For PdRe catalysts, assume 2.0 H/Pd with the balance to Re^{7+} reduction. ³ Based on TPR H_2 consumption by Pd3-TA after reduction and passivation. ⁴ Based on H_2 evolution at >0°C.

The TPR profiles of bimetallic catalysts prepared using HReO_4 and $\text{Pd}(\text{NO}_3)_2$ are qualitatively similar (Figure 2b). An extremely sharp peak attributed to reduction of PdO crystallites is observed at $\sim 25^\circ\text{C}$. Although similar to the low-temperature TPR peak observed for Pd3-N, it occurs at $\sim 20^\circ\text{C}$ higher temperature. A second low-temperature TPR peak appears at $\sim 55\text{--}60^\circ\text{C}$ that may be assigned to Pd or Re species. The higher temperature ($>100^\circ\text{C}$) TPR features are consistent with Re reduction. The maximum rate of H_2 consumption occurs at $\sim 260^\circ\text{C}$ —more than 100°C below the peak reduction temperature of Re5-N. Facilitated reduction of perrhenate species in $\text{PdRe}/\text{Al}_2\text{O}_3$ catalysts has been ascribed to (i) hydrogen spillover from Pd particles [21] and (ii) migration of Re_2O_7 to Pd particles in the presence of adsorbed H_2O [18]. In contrast to Re5-N, TPR of Pd3Re5-CI evidences that essentially all supported Re has been reduced after heating to 400°C in 5% H_2/Ar (Table 2).

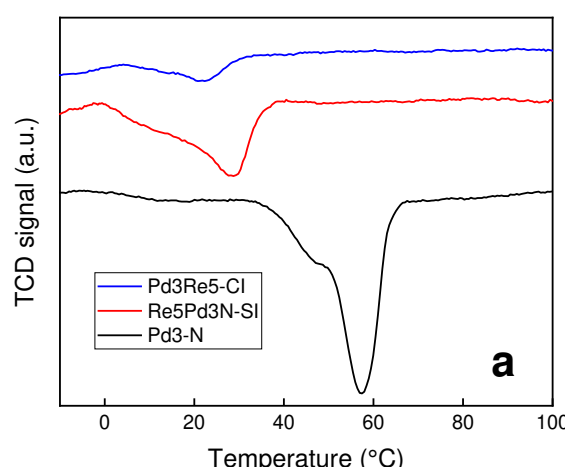
The bimetallic catalysts Re5Pd3-SI and Re5Pd3-SI (350) have similar TPR profiles (Figure 2c) comprising a sharp Pd reduction peak at $\sim 10^\circ\text{C}$ and a broad Re reduction feature at 30–200°C. The Pd reduction peak is sharper and occurs at lower temperature than for Pd3-TA (A) suggesting that the presence of supported perrhenate species affects Pd^{2+} reduction. Most Re reduction occurs at <200°C consistent with hydrogen spillover from highly dispersed Pd particles [21]. Essentially complete Re reduction is obtained for both catalysts at 400°C (Table 2). Increasing the calcination temperature to 400°C and time to 3 h sharpens the peaks and lowers the Re reduction temperature. The converse would be expected for moisture-dependent diffusion of ReO_x species to Pd^0 particles. The TPR profile of Pd3Re5-SI exhibits a single symmetric peak with a maximum at $\sim 80^\circ\text{C}$. Ziemecki, et al. reported a similar TPR profile (47°C peak maximum) for a $\text{PdRe}/\text{Al}_2\text{O}_3$ catalyst prepared by impregnation of a reduced 3 wt.% $\text{Pd}/\text{Al}_2\text{O}_3$ catalyst with aqueous Re_2O_7 and dehydration at 110°C [18]. Malinowski, et al. [13] also reported complete reduction of similarly prepared $\text{PdRe}/\text{Al}_2\text{O}_3$ catalysts after heating H_2

at 400°C for 3 h. Ziemecki, et al. inferred that Re_2O_7 mobility on the hydroxylated $\gamma\text{-Al}_2\text{O}_3$ surface was the underlying mechanism of low-temperature Re reduction, because dehydroxylation at 500°C caused reduction to occur at much higher temperatures and PdRe alloy particles were formed [18].

Quantitative H_2 uptake measurements on the bimetallic catalysts indicate that >90% of the Re was reduced to the zero-valent state after TPR to 400°C (Table 2). Residual Re^{7+} species interacting strongly with the support and intermediate Re oxidation states (e.g., Re^{4+}) cannot be completely excluded.

TPHD measurements were performed on the 3 wt.% Pd/ Al_2O_3 catalysts after TPR to 400°C. The TPHD spectrum of Pd3-N comprises a sharp H_2 evolution peak at ~55°C with a shoulder at ~50°C. The H/Pd ratio (Table 2) is approximately half that observed in bulk Pd (H/Pd = 0.65) under similar conditions [17,18]. In contrast, the TPHD spectrum of Pd3-TA comprises a broad asymmetric H_2 evolution peak centered around ~30°C and a small sharp peak at ~55°C. The H/Pd ratio is less than half that for Pd3-N (Table 2) consistent with highly dispersed supported Pd [35]. We assign the broad low-temperature peak to decomposition of supported PdH_x nanoparticles and the small peak at 55°C to larger supported Pd crystallites. A lower decomposition temperature indicates lower stability of the PdH_x phase in supported nanoparticles.

Re addition via any of the methods employed herein alters the H/Pd ratio and stability of the bulk PdH_x phase. Alloying Pd with other transition metals (e.g., Au) is known to alter its electronic structure and destabilize the bulk hydride phase. The highest concentration of Re in PdRe solid solutions is ~10% [36]; however, bulk thermodynamics may not apply to small particles [37]. Ziemecki, et al. employed H_2 uptake during cooling in the TPR apparatus to assess hydride suppression and infer alloy formation in PdAu and PdRe catalysts [17]. Malinowski, et al. [13] used a second TPR (equivalent to our TPHD) to characterize PdRe/ Al_2O_3 catalysts and reported a reduction in H/Pd ratio and destabilization of the hydride phase with increasing Re content. TPHD measurements on bimetallic catalysts prepared by using $\text{Pd}(\text{NO}_3)_2$ are shown in Figure 3a. For both catalysts, there is a significant reduction in Pd/H ratio (Table 2) and low-temperature shift in decomposition temperature relative to Pd3-N. These observations are consistent with a strong PdRe bulk interaction, i.e., alloy formation in Pd-rich particles. TPHD spectra of more highly dispersed bimetallic catalysts are shown in Figure 3b. PdH_x formation is completely suppressed in the 2:1 Re:Pd (bulk atomic ratio) catalyst prepared from the DCS [38]. The TPHD spectrum of Pd3Re5-SI suggests a strong PdRe interaction; hydride formation is strongly suppressed and decomposition occurs at much lower temperatures than typical for PdH_x nanoparticles. Ziemecki, et al. reported equivalent observations for a similarly prepared PdRe/ Al_2O_3 catalyst lending support to the Re_2O_7 surface mobility hypothesis [18]. In contrast, the TPHD spectra of Re5Pd3-SI and Re5Pd3-SI (350) contain a single sharp decomposition peak at 40-50°C consistent with PdH_x particles, and the H/Pd ratios (Table 2) are equivalent to that of Pd3-TA. These results do not suggest bulk alloy formation and are consistent with low-temperature Re reduction via hydrogen spillover from vicinal Pd nanoparticles.



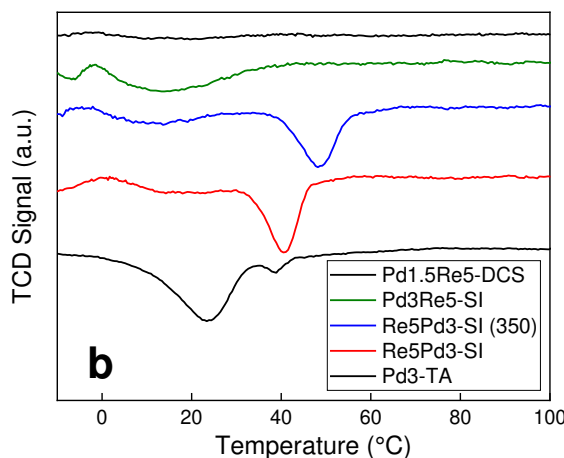


Figure 3. TPHD spectra for catalysts after TPR to 400°C and cooling in 5% H₂/Ar.

CO and H₂ chemisorption data are provided in Table 3. The data confirm that Pd3-TA is more highly dispersed than Pd3-N, as expected from Raman spectroscopy and TPR. The CO/Pd ratio for Pd1-N is approximately three times higher than for Pd3-N indicating that lowering the Pd loading increases dispersion, as expected. At 35°C, the H/CO ratios are approximately unity for Pd3-N and Pd1-N. H₂ chemisorption uptake declined by ~30% for these catalysts at 100°C. The low CO/Re ratio for Re5-N is consistent with previous volumetric chemisorption data on Re/Al₂O₃ [2016]. The H/CO ratio for Re5-N at 35°C is only ~15%, but H₂ uptake increases at 100°C consistent with activated dissociative chemisorption [39].

Table 3. CO and H₂ chemisorption results.

Catalyst	CO chemisorption			H ₂ chemisorption				H/CO	
	35°C		35°C		100°C				
	CO uptake ^a	CO/metal	H ₂ uptake ^a	H/metal	H/CO	H ₂ uptake	H/metal		
Pd1-N	28.5	0.333	12.7	0.297	0.89	8.8	0.204	0.62	
Pd3-N	32.4	0.130	16.7	0.133	1.03	12.4	0.100	0.76	
Pd3-TA	103	0.469	n/a	--	--	n/a	--	--	
Pd3Re5-CI	59.0	0.127	26.7	0.115	0.90	27.3	0.117	0.92	
Pd3Re5-SI	80.5	0.157	17.9	0.070	0.44	21.6	0.084	0.54	
Re5Pd3N-SI	50.5	0.099	n/a	--	--	n/a	--	--	
Re5Pd3-SI (350)	96.2	0.206	20.9	0.089	0.43	26.7	0.114	0.56	
Re5Pd3-SI	92.6	0.210	20.3	0.092	0.44	21.1	0.096	0.46	
Pd1.5Re5-DCS	44.6	0.116	7.6	0.040	0.34	11.0	0.057	0.49	
Re5-N	33.8	0.139	2.3	0.019	0.14	14.5	0.119	0.86	

^a units: $\mu\text{mol/g}$.

The CO uptakes of Pd3Re5-CI and Re5Pd3N-SI are greater than Pd3-N indicating either a significant Re-CO contribution and/or smaller Pd particle size. In contrast, Pd3Re5-SI has lower CO uptake than Pd3-TA notwithstanding Re addition. The CO uptakes for Re5Pd3-SI and Re5Pd3-SI (350) are only ~10% lower than Pd3-TA. H₂ chemisorption is strongly suppressed (relative to CO chemisorption) on the Pd3Re5-SI, Re5Pd3-SI, Re5Pd3-SI (350) and Pd1.5Re5-DCS catalysts suggesting Re coverage of the supported Pd particles. Re addition to Pd/Al₂O₃ catalysts is known to suppress H₂ chemisorption [13,14], and we have provided evidence that Re blocks surface sites on Pd particles [21]. The H/CO ratios observed for the bimetallic catalysts in this work, except Pd3Re5-CI, are ~0.4 at 35°C and ~0.5 at 100°C consistent with suppression of H₂ chemisorption. The chemisorptive properties of Pd3Re5-CI are more consistent with supported Pd than a bimetallic catalyst.

In general, the Kubelka-Munk (K-M) intensities of the CO DRIFT spectra are consistent with the CO chemisorption uptakes ($\mu\text{mol/g}_{\text{cat}}$) of the catalysts. Catalysts prepared using Pd tetraammine (including the DCS) (Figure 4a) have more intense $\nu(\text{CO})$ peaks than catalysts prepared from $\text{Pd}(\text{NO}_3)_2$ (Figure 4b). For Pd3-TA, the linear (atop) CO peak ($\sim 2080 \text{ cm}^{-1}$) is more intense than the broad bridging CO band ($\sim 1930 \text{ cm}^{-1}$) consistent with highly dispersed supported Pd [40–42]. The 1930-cm^{-1} band and its low-frequency tail (extending to 1700 cm^{-1}) are associated with doubly and triply bridging CO species on Pd nanoparticles. The CO DRIFT spectrum of Re5Pd3-SI is closely similar albeit of lower intensity. A significant enhancement of the linear-to-bridging (L/B) ratio and a blueshift of the bridging CO band to $\sim 1950 \text{ cm}^{-1}$ are observed for Pd3Re5-SI. We infer that these trends indicate surface modification by Re adatoms leaving fewer adjacent Pd atoms to accommodate bridging CO species. The CO DRIFT spectrum of Pd1.5Re5-DCS is qualitatively similar, but the peak intensities are much lower consistent with its lower Pd loading. Only a small shoulder at $\sim 2040 \text{ cm}^{-1}$ assigned to CO linearly adsorbed on metallic Re particles is observed for these catalysts [38,43]. There are several potential explanations: $[\text{ReO}_4]^-$ (or Re_2O_7) species spread over the $\gamma\text{-Al}_2\text{O}_3$ surface during calcination [54], and reduction of isolated $[\text{ReO}_4]^-$ species is incomplete at 400°C . Alternatively, re-oxidation of Re metal centers (single atoms, clusters) can occur during the He purge at 400°C after *in situ* reduction [38,44].

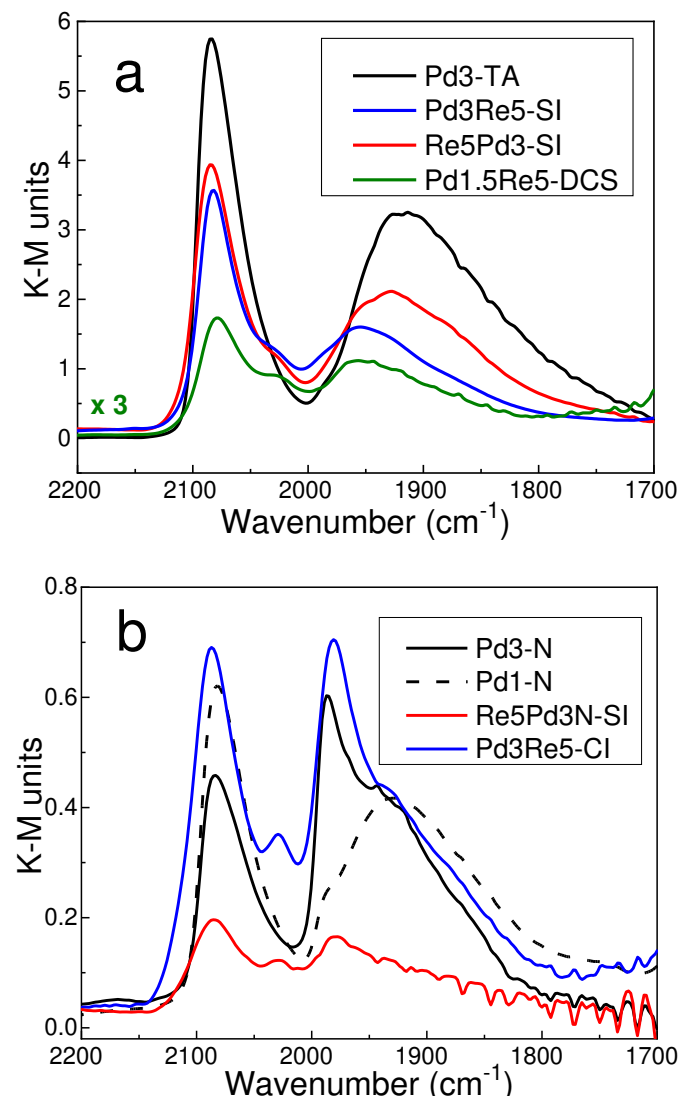


Figure 4. DRIFT spectra of adsorbed CO at 20°C on $\text{Pd}/\text{Al}_2\text{O}_3$ and $\text{PdRe}/\text{Al}_2\text{O}_3$ catalysts following *in situ* H_2 reduction at 400°C .

The CO DRIFT spectrum of Pd3-N comprises linear and bridging bands (Figure 4b), and the latter are dominant. The prominent 1990-cm⁻¹ peak corresponds to bridging CO on low-index surface planes [e.g., (100) and (111)] of supported Pd crystallites [41,42]. The strong shoulder at 1930 cm⁻¹ is equivalent to that observed for supported Pd nanoparticles (Figure 4a). For Pd1-N, conversely, there is only a medium shoulder at 1990 cm⁻¹, and the 1930-cm⁻¹ bridging band is more prominent. The L/B ratio is also higher consistent with its higher dispersion. The CO DRIFT spectrum of Pd3Re5-CI contains strong peaks at 2080 and 1990 cm⁻¹ assigned to linear and doubly bridging CO, and the L/B ratio is higher when compared to Pd3-N. A medium-intensity peak at ~2040 cm⁻¹ is assigned to linear CO on Re [38,43]. We infer that coverage of Pd particles by Re (or alloying) results in fewer adjacent Pd atoms exposed, thereby increasing the L/B ratio. The CO DRIFT spectrum of Re5Pd3N-SI is qualitatively similar with linear and bridging Pd-CO bands and a small linear Re-CO peak at ~2040 cm⁻¹.

Low-magnification HAADF-STEM images of Pd3Re5-SI and Re5Pd3-CI catalyst particles (Figure 5) provide visual evidence of the much higher metal dispersion and more uniform distribution in the former. Small bright scattering centers (metal particles) are observed uniformly covering the γ -Al₂O₃ support in Figure 5a. In contrast, larger metal particles are seen near the particle edges in Figure 5b. Figure 6a displays a higher magnification HAADF image of Pd3Re5-CI showing two large (20-30 nm) and many small metal particles (<5 nm) distributed across the support. The composite EDX image (Figure 6b) clearly identifies the small particles as Re, whereas the two large particles (crystallites) contain primarily Pd. The intense yellow pixels associated with the Pd particles result from superposition of red (Pd) and green (Re) pixels. Although this image provides no depth resolution, it is clear that there are patches of Re (or ReO_x) on the larger Pd particles. Based on the TPHD results for Pd3Re5-CI (strong suppression of bulk hydride formation), it is probable that the larger bimetallic particles are alloyed. Much smaller (<5 nm) segregated Re and Pd particles are found in other regions of the γ -Al₂O₃ support, as illustrated in Figure 6c,d.

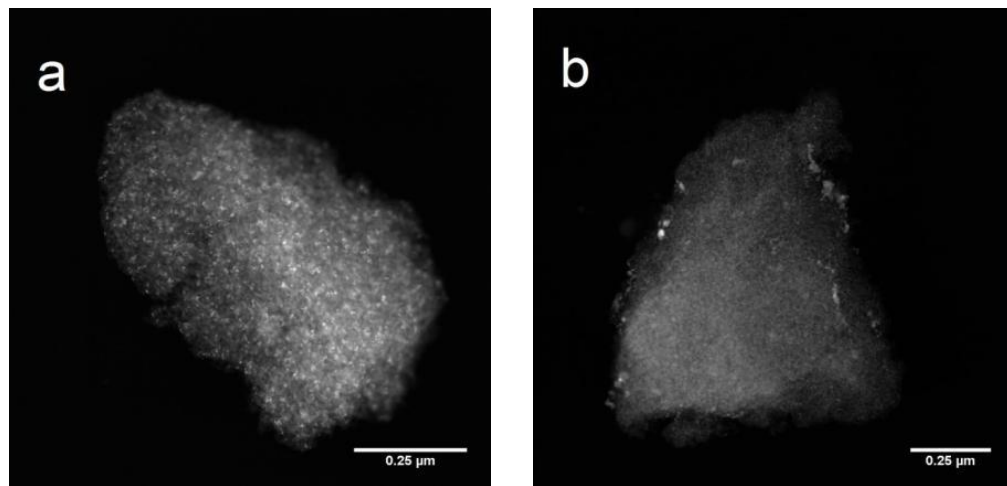


Figure 5. Low-magnification HAADF-STEM images of individual catalyst particles: (a) Re5Pd3-SI and (b) Pd3Re5-CI.

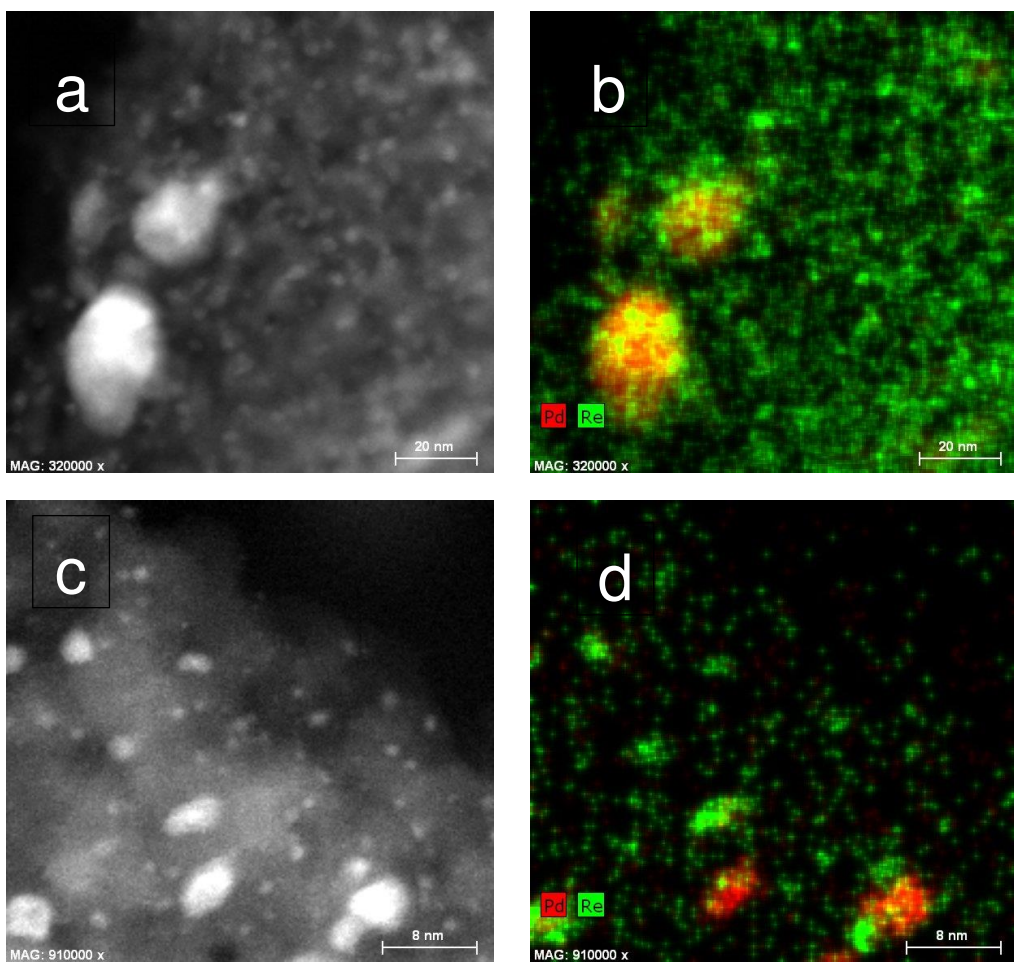
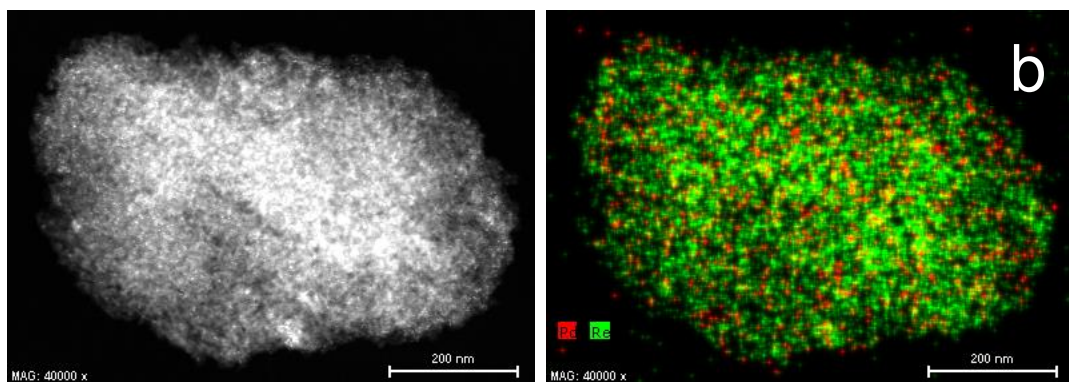


Figure 6. STEM images of Pd₃Re₅-Cl: HAADF images (**a,c**) and composite EDX images (**b,d**). Colors: red—Pd, green—Re, yellow—superposition.

The HAADF image and EDX maps of another Re₅Pd₃-SI particle (Figure 7) reveal remarkably uniform distributions of Pd and Re nanoparticles on the γ -Al₂O₃ support. The Pd particles appear discrete, whereas the Re coverage appears nearly continuous. The supported nanoparticles are <5 nm in size, as seen in the high magnification HAADF image in Figure 8a. The EDX map (Figure 8b) suggests that Pd and Re are segregated within the supported bimetallic nanoparticles—consistent with the TPHD results indicating no suppression of hydride formation.



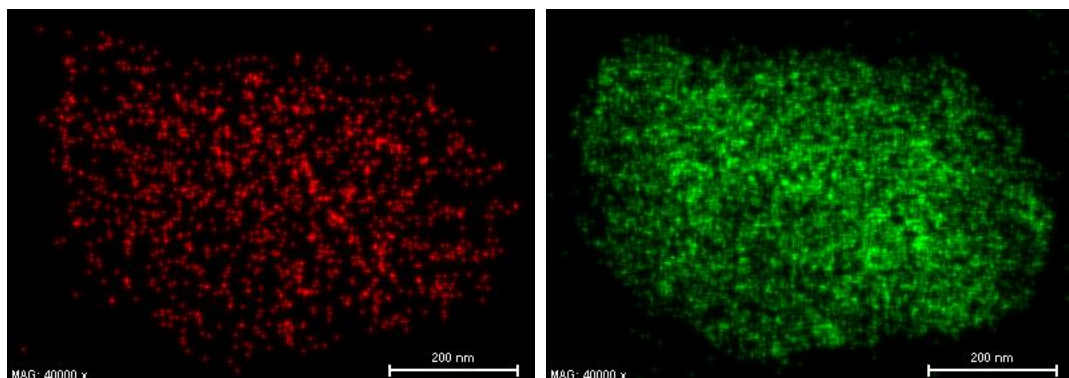


Figure 7. STEM of Re5Pd3-SI catalyst: HAADF image (a), composite EDX map (b), Pd EDX map (c) and Re EDX map (d).

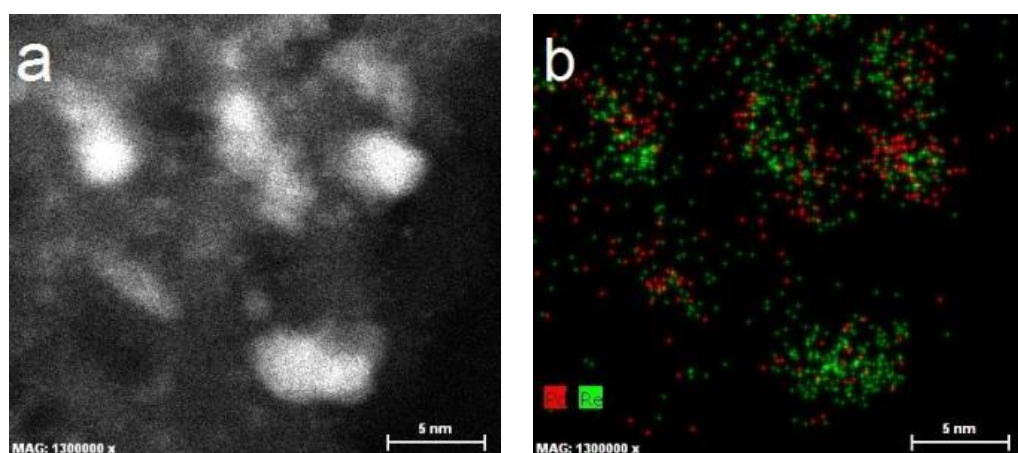


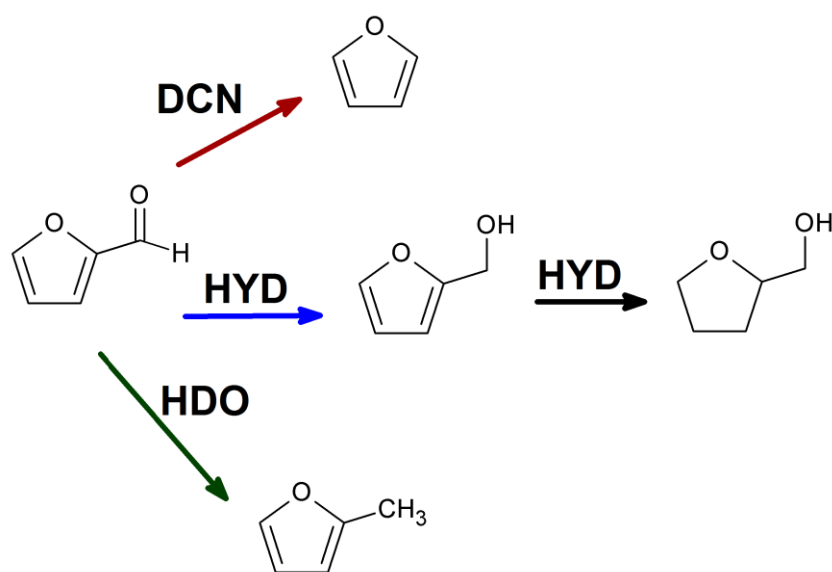
Figure 8. High-magnification STEM of Re5Pd3-SI catalyst: HAADF image (a) and corresponding EDX map (b) showing Pd (red) and Re (green).

2.2. Furfural hydrogenation catalysis

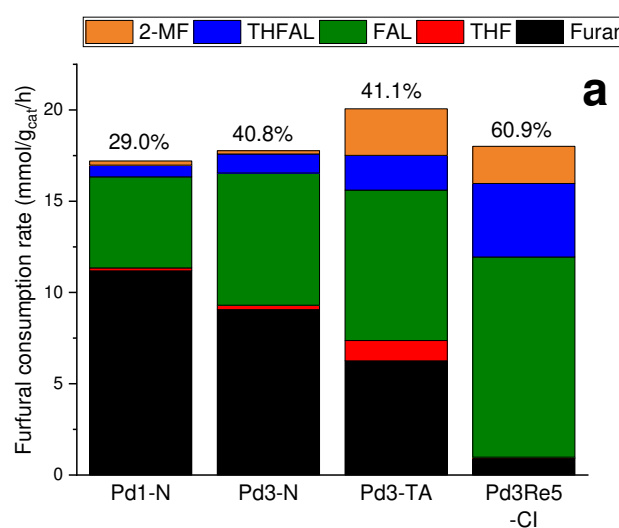
Three reaction pathways were inferred for furfural conversion over Pd/Al₂O₃ and PdRe/Al₂O₃ catalysts under the investigated conditions (Scheme 1). Ring-opening products (e.g., butanols and pentanols) were not observed. Furan (F), furfuryl alcohol (FAL), and tetrahydrofurfuryl alcohol (THFAL) were identified as primary products over Pd/Al₂O₃ via the Delplot method [21]. Furfural decarbonylation (DCN) produces F and CO. Selective hydrogenation (HYD) to FAL is the desired pathway. A third pathway is direct hydrodeoxygenation (HDO) to 2-methylfuran (2-MF). 2-MF was a primary product only over Pd3-N and the Re-containing catalysts. Selectivity to other ring-saturation products: tetrahydrofuran (THF) and 2-methyl THF (2-MTHF) was generally low indicating secondary products. Re5-N was essentially inactive relative to the Pd/Al₂O₃ and PdRe/Al₂O₃ catalysts.

Product formation rates for the Pd/Al₂O₃ and PdRe/Al₂O₃ catalysts are shown in Figure 9; the total bar height represents the furfural consumption rate for each catalyst. The Pd/Al₂O₃ catalysts (irrespective of precursor) and Pd3Re5-CI (Figure 9a) were far less active than the bimetallic catalysts prepared from the DCS and by SI (Figure 9b). The higher activities of the latter are likely because of their higher metal dispersions. The similar activities of the Pd3-N and Pd3-TA catalysts are surprising given the much higher dispersion of the latter. Furan was the main product over the Pd1-N and Pd3-N catalysts, and the order of relative abundance was: F + THF > FAL + THFAL >> 2-MF. Over Pd3-TA, the order was FAL + THFAL > F + THF > 2-MF showing a modest preference for aldehyde group HYD over DCN. Interestingly, F production was suppressed markedly over all the bimetallic catalysts regardless of activity. For example, the Pd3-N and Pd3Re5-CI catalysts both have similar low activities, but the latter has much greater FAL selectivity and far lower F selectivity. All the

bimetallic catalysts strongly favored HYD over DCN with the order of relative product abundance: FAL + THFAL >> F + THF ~ 2-MF. This product distribution is more consistent with Re (rather than Pd) catalysis. The DCS-derived catalyst was most selective to FAL (78.3%) and exhibited 93% selectivity to FAL + THFAL. The Pd3Re5-SI and Re5Pd3-SI (350) catalysts had similar activities and FAL selectivities indicating that the impregnation sequence is relatively unimportant. The Re5Pd3-SI catalyst (that was calcined at 400°C for 3 h after each impregnation step) was more active but less selective to FAL; however, its FAL + THFAL selectivity (81%) was comparable to the other SI catalysts. The Pd3Re5-SI catalyst prepared from the $\text{Pd}(\text{NH}_3)_4(\text{NO}_3)_2$ precursor was more active and more selective than a SI catalyst derived from $\text{Pd}(\text{NO}_3)_2$ reported previously [21]. The Re-first SI and the DCS-derived catalysts are modestly (~20%) more active with ~10% greater FAL selectivity than those reported previously [21]. We speculate that this could be a promoter effect of the Group I or IIA metal impurities in $\gamma\text{-Al}_2\text{O}_3$ (A) [11].



Scheme 1. Furfural catalytic reaction pathways: decarbonylation (DCN), hydrogenation (HYD), and hydrodeoxygenation (HDO). Only primary products are shown.



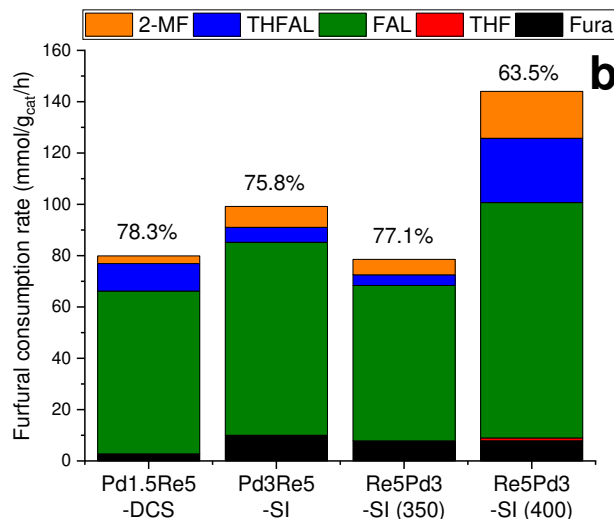


Figure 9. Furfural consumption rates and product formation rates at 150°C and 1 atm at differential (<10%) conversion. FAL selectivities are indicated above the bars.

Turnover frequencies (TOFs) for furfural consumption at 150°C are given in Table 4. The TOF(CO) values (based on CO adsorption isotherms measured at 35°C) are in excellent agreement for the Pd1-N and Pd3-N catalysts and in good agreement with those previously reported for Pd/Al₂O₃ catalysts [21]. Moreover, their TOF(H) values (per H atom based on H₂ dissociative chemisorption at 35°C) are also in excellent agreement (with each other and the TOF(CO) values). Overall, the TOF(CO) values of the PdRe/Al₂O₃ catalysts (except Pd3Re5-CI) are 2-5 times higher than those of the Pd/Al₂O₃ catalysts. TOF(H) values (per H atom based on H₂ dissociative chemisorption at 100°C) are approximately two times higher than TOF(CO) values over the PdRe/Al₂O₃ catalysts (except Pd3Re5-CI). The TOFs for Pd3Re5-CI are lower and in better agreement with those of the Pd/Al₂O₃ catalysts. The TOFs for Pd3Re5-SI agree very closely with those reported previously for an analogous catalyst prepared using a 3 wt.% Pd/Al₂O₃ catalyst derived from Pd(NO₃)₂ [21]. Finding equivalent TOFs despite large differences in Pd dispersion validates using CO and H₂ chemisorption for counting active sites. Both SI methods produce highly active and selective catalysts. The highly dispersed PdRe/Al₂O₃ prepared by impregnation with the DCS exhibits the highest intrinsic activity and FAL selectivity. We infer that intimate contact between supported Pd and Re nanoparticles results in suppression of Pd-catalyzed decarbonylation and creates Pd-Re sites with high intrinsic activity. Our results are consistent with the proposal that Pd facilitates the reaction via H₂ dissociation and spillover of H species onto Re sites [22].

Table 4. TOFs for furfural consumption at 150°C measured under differential conversion (<10%) conditions.

Catalyst	TOF (min ⁻¹) ^a	
	CO	H
Pd1-N	10.1	11.3 ^b
Pd3-N	9.1	8.9 ^b
Pd3-TA	3.2	n/a
Pd3Re5-CI	5.1	5.5
Pd3Re5-SI	20.5	38.3
Re5Pd3-SI (350)	13.6	24.5
Re5Pd3-SI	26.0	57.0
Pd1.5Re5-DCS	29.9	60.6

^a Basis: CO chemisorption at 35°C and H₂ dissociative chemisorption at 100°C (unless otherwise noted). ^b Basis: H₂ dissociative chemisorption at 35°C.

3. Materials and Methods

3.1. Catalyst Preparation

The γ -Al₂O₃ support (BET surface area and total pore volume of 217 m²/g and 0.47 cm³/g, respectively) was purchased from Strem Chemicals. Elemental analysis by inductively coupled plasma-optical emission spectrometry (ICP-OES) revealed the following alkali metal and alkaline earth metal impurities: 213 ppm Na, 24.0 ppm Mg, 8.32 ppm K, and 132 ppm Ca. The mono- and bimetallic catalysts were prepared by IW impregnation, except for the Pd1.5Re5-DCS catalyst which was prepared by wet impregnation with [Pd(NH₃)₄(ReO₄)₂], as described elsewhere [38]. For the bimetallic catalysts, 3 different IW methods and precursors were employed: (i) co-impregnation using Pd(NO₃)₂ and HReO₄, (ii) Re-first sequential impregnation using NH₄ReO₄ and [Pd(NH₃)₄(NO₃)₂], and (iii) HReO₄ addition to a reduced and passivated Pd/Al₂O₃ catalyst. These methods are described in more detail elsewhere [21]. For comparison, a catalyst (Re5Pd3N-SI) was also prepared by Re-first sequential impregnation using HReO₄ and Pd(NO₃)₂. The Pd tetraammine nitrate, Pd(NO₃)₂, and Pd(NO₃)₂ + HReO₄ impregnation solutions were pH 10, pH 7, and pH 1, respectively. The Typically, after each impregnation step, catalysts were dried at 110°C overnight, crushed with mortar and pestle, and calcined at 400°C for 3 h in flowing zero-grade air. The Pd1.5Re5-DCS and Pd3Re5-SI catalysts were not calcined. All catalysts were stored in a desiccator prior to use. ICP-OES analysis for Pd and Re was performed by Eastman Chemical Company (Kingsport, TN).

3.2. TPR and TPHD

TPR and TPHD experiments were performed using a Micromeritics 2920 Autochem II equipped with a thermal conductivity detector (TCD) for monitoring H₂ uptake/evolution. Catalyst samples (100 mg) were cooled to -50°C in ultra-high purity He (National Welders), and the feed gas was switched to 5% H₂/Ar (certified mixture, Machine and Welding Supply). Both gases were purified using inline H₂O/O₂ traps (Oxilab). After waiting for TCD baseline to stabilize, the sample was heated at 10°C/min to 400°C and held for 1 h. Select Re-containing catalysts were heated to 800°C to ensure complete reduction was achieved. After TPR to 400°C, Pd-containing catalysts were cooled to -50°C in 5% H₂/Ar and purged with Ar. Subsequently, TPHD spectra were measured using the TCD and a temperature ramp of 10°C/min to 400°C in flowing Ar.

3.3. CO and H₂ Chemisorption

Volumetric H₂ and CO chemisorption measurements were performed using a Micromeritics ASAP 2020c instrument. Each catalyst was reduced *in situ* in flowing research-grade H₂ (50 sccm) at 400°C for 1 h, evacuated at 400°C for 2 h using a turbomolecular pump, then cooled to 100°C for H₂ analysis. Adsorption isotherms were measured before and after evacuation at the analysis temperature; the difference was used to determine strongly adsorbed species. The H₂ analysis was repeated at 70°C and 35°C, and the sample was evacuated at 300°C for 1 h between each analysis. Subsequently, CO adsorption isotherms were measured at 35°C.

3.4. CO DRIFTS

DRIFT spectra of adsorbed CO were measured on a Bruker Vertex 70 FTIR with a liquid N₂-cooled MCT detector using a Harrick Praying Mantis cell. Prior to measurement, samples were reduced in *in situ* the DRIFTS cell at 400°C for 1 h in 40 sccm H₂ (research grade, National Welders), then purged in He at 40 sccm (UHP, National Welders) for 1 h before cooling to 20°C. Pulses of 5% CO/He (certified, National Welders) were administered five at a time at 20°C until no further changes in spectra were observed. Scans of the reduced catalyst (128 scans at 4 cm⁻¹ resolution) at 20°C in He were subtracted from scans following pulses of CO in order to subtract out signal from H₂O.

3.5. Raman Spectroscopy

Raman spectra of the powder samples were recorded on a Horiba Jobin-Yvon LabRAM HR VIS high-resolution confocal Raman microscope using a He-Ne laser (632 nm) excitation source and 100X objective. The laser power was 20 mW, and the confocal hole size was 800 μm . The instrument was calibrated using a Si wafer at 520.7 cm^{-1} . The exposure time was 15 s at a resolution of 0.1 cm^{-1} . Catalyst samples were removed the storage desiccator and handled and scanned in ambient air. No spectral degradation was observed during data collection. Raman bands due to the $\text{o-Al}_2\text{O}_3$ support were removed by spectral subtraction.

3.6. HAADF-STEM-EDX

High-resolution STEM imaging was performed on an aberration-corrected FEI Titan 80-300 electron microscope. The microscope is equipped with a high-angle annular dark field (HAADF) detector and SuperX EDS system comprising four Bruker silicon drift detectors. Samples were reduced *ex situ* at 400°C, and handled under N_2 , except for brief exposure during insertion into the microscope. The powder was supported on carbon-coated copper grids (Ted Pella).

3.7. Furfural hydrogenation

Furfural hydrogenation activity was tested in a continuous flow packed-bed reactor system at 150°C and atmospheric pressure. The catalyst bed comprised 50-250 mg catalyst powder and 1.25 g quartz chips and was supported by quartz wool in a 0.5" stainless steel tube. Catalyst bed temperature was measured by a Type-K thermocouple (Omega) in contact with the catalyst inside the tube. Furfural was fed by a syringe pump, vaporized in a stream of 100% H_2 , and passed over the catalyst bed. The effluent was monitored by two on-line gas chromatographs (GCs): GC-TCD (SRI 8610C) with a ShinCarbon ST100 (2 m x 1.0 mm ID) column (Restek) measured CO, CH_4 and CO_2 ; a GC-FID (Shimadzu 2010) with an EconoCap-1 column (30 m x 0.53 mm ID, Alltech) measured all other products.

4. Conclusions

Highly dispersed PdRe/ Al_2O_3 catalysts for selective hydrogenation of furfural combine synergistically: (1) inhibition of Pd-catalyzed decarbonylation by Re and (2) promotion of Re hydrogenation activity via intimate contact with Pd. Optimum catalysts comprise supported bimetallic nanoparticles; bulk alloy formation is not required. A low-dispersion PdRe/ Al_2O_3 catalyst containing supported Pd-Re alloy crystallites exhibited a furfural TOF similar to Pd/ Al_2O_3 albeit with higher FAL selectivity.

Acknowledgements: This work was funded by Eastman Chemical Company for funding through the Center of Excellence at North Carolina State University. ICP-OES analysis was performed by Eastman Chemical Company. The authors acknowledge the use of the Analytical Instrumentation Facility at NCSU, which is supported by the State of North Carolina and the National Science Foundation, and, in particular, Dr. Xiaohan Sang for assistance with STEM-EDX.

References

1. K.Y. Chen, S. Koso, T. Kubota, Y. Nakagawa, K. Tomishige, *Chemcatchem*, **2** (2010) 547-555.
2. S. Koso, Y. Nakagawa, K. Tomishige, *J. Catal.*, **280** (2011) 221-229.
3. M. Chia, Y.J. Pagan-Torres, D. Hibbitts, Q.H. Tan, H.N. Pham, A.K. Datye, M. Neurock, R.J. Davis, J.A. Dumesic, *J. Am. Chem. Soc.*, **133** (2011) 12675-12689.
4. S. Koso, I. Furikado, A. Shima, T. Miyazawa, K. Kunimori, K. Tomishige, *Chem. Comm.*, (2009) 2035-2037.
5. L. Ma, D.H. He, Z.P. Li, *Catal. Comm.*, **9** (2008) 2489-2495.
6. L. Ma, D.H. He, *Top. Catal.*, **52** (2009) 834-844.
7. Y. Takeda, Y. Nakagawa, K. Tomishige, *Catal. Sci. Tech.*, **2** (2012) 2221-2223.
8. A. Shima, S. Koso, N. Ueda, Y. Shinmi, I. Furikado, K. Tomishige, *Chem. Lett.*, **38** (2009) 540-541.
9. S. Koso, H. Watanabe, K. Okumura, Y. Nakagawa, K. Tomishige, *J. Phys. Chem. C*, **116** (2012) 3079-3090.

10. B.K. Ly, D.P. Minh, C. Pinel, M. Besson, B. Tapin, F. Epron, C. Espezel, *Top. Catal.*, **55** (2012) 466-473.
11. M.A. Mabry, W.W. Prichard, S.B. Ziemecki, in, E. I. du Pont de Nemours and Company, United States Patent 4550185, 1985.
12. M. Kitson, P.S. Williams, in: U.S.P. Office (Ed.), The British Petroleum Company, United States Patent 5149680, 1992.
13. A. Malinowski, W. Juszczysz, M. Bonarowska, J. Pielaszek, Z. Karpinski, *J. Catal.*, **177** (1998) 153-163.
14. M. Bonarowska, A. Malinowski, Z. Karpinski, *Appl. Catal. A*, **188** (1999) 145-154.
15. W. Juszczysz, Z. Karpinski, *App. Catal. A*, **206** (2001) 67-78.
16. G. Meitzner, G.H. Via, F.W. Lytle, J.H. Sinfelt, *J. Chem. Phys.*, **87** (1987) 6354-6363.
17. S.B. Ziemecki, J.B. Michel, G.A. Jones, *React. Sol.*, **2** (1986) 187-202.
18. S.B. Ziemecki, G.A. Jones, J.B. Michel, *J. Catal.*, **99** (1986) 207-217.
19. M.P. Latussek, B.P. Spigarelli, R.M. Heimerl, J.H. Holles, *J. Catal.*, **263** (2009) 306-314.
20. M.D. Skoglund, J.H. Holles, *Catal. Lett.*, **143** (2013) 966-974.
21. S.T. Thompson, H.H. Lamb, *ACS Catal.*, **6** (2016) 7438-7447.
22. J.D. Kammert, A. Chemburkar, N. Miyake, M. Neurock, R.J. Davis, *ACS Catal.*, **11** (2021) 1435-1455.
23. K. Otto, C.P. Hubbard, W.H. Weber, G.W. Graham, *App. Catal. B*, **1** (1992) 317-327.
24. A. Baylet, P. Marecot, D. Duprez, P. Castellazzi, G. Groppi, P. Forzatti, *Phys. Chem. Chem. Phys.*, **13** (2011) 4607-4613.
25. F.D. Hardcastle, I.E. Wachs, J.A. Horsley, G.H. Via, *J. Mol. Catal.*, **46** (1988) 15-36.
26. M.A. Vuurman, I.E. Wachs, *J. Phys. Chem.*, **96** (1992) 5008-5016.
27. D.S. Kim, I.E. Wachs, *J. Catal.*, **141** (1993) 419-429.
28. J.R. McBride, K.C. Hass, W.H. Weber, *Phys. Rev. B*, **44** (1991) 5016-5028.
29. S.C. Su, J.N. Carstens, A.T. Bell, *J. Catal.*, **176** (1998) 125-135.
30. A.S. Mamede, G. Leclercq, E. Payen, P. Granger, J. Grimblot, *J. Mol. Struc.*, **651** (2003) 353-364.
31. T. Arai, T. Shima, T. Nakano, J. Tominaga, *Thin Sol. Films*, **515** (2007) 4774-4777.
32. L. Jiao, J.R. Regalbuto, *J. Catal.*, **260** (2008) 329-341.
33. J. Okal, L. Kepinski, L. Krajczyk, W. Tylus, *J. Catal.*, **219** (2003) 362-371.
34. C. Sumner, W. Burchett, *Top. Catal.*, **55** (2012) 480-485.
35. J.A. McCaulley, *J. Phys. Chem.*, **97** (1993) 10372-10379.
36. B. Predel, O.E. Madelung, in: Landolt-Börnstein - Group IV Physical Chemistry, SpringerMaterials.
37. J.H. Sinfelt, Bimetallic Catalysts: Discoveries, Concepts, and Applications, John Wiley and Sons, 1983.
38. S.T. Thompson, H.H. Lamb, *J. Catal.*, **350** (2017) 111-121.
39. G.W. Chadzynski, H. Kubicka, *Thermochim. Acta*, **158** (1990) 353-367.
40. J.B. Giorgi, T. Schroeder, M. Baumer, H.J. Freund, *Surf. Sci.*, **498** (2002) L71-L77.
41. G. Agostini, R. Pellegrini, G. Leofanti, L. Bertinetti, S. Bertarione, E. Groppo, A. Zecchina, C. Lamberti, *J. Phys. Chem. C*, **113** (2009) 10485-10492.
42. T. Lear, R. Marshall, J.A. Lopez-Sanchez, S.D. Jackson, T.M. Klapotke, M. Baumer, G. Rupprechter, H.J. Freund, D. Lennon, *J. Chem. Phys.*, **123** (2005) 13.
43. W. Daniell, T. Weingand, H. Knozinger, *J. Mol. Catal.*, **204** (2003) 519-526.
44. S.R. Bare, S.D. Kelly, F.D. Vila, E. Boldingh, E. Karapetrova, J. Kas, G.E. Mickelson, F.S. Modica, N. Yang, J.J. Rehr, *J. Phys. Chem. C*, **115** (2011) 5740-5755.

Disclaimer/Publisher's Note: The statements, opinions and data contained in all publications are solely those of the individual author(s) and contributor(s) and not of MDPI and/or the editor(s). MDPI and/or the editor(s) disclaim responsibility for any injury to people or property resulting from any ideas, methods, instructions or products referred to in the content.